Biochemical Pharmacology 250 (2026) 117998

Contents lists available at ScienceDirect

Biochemical Pharmacology

journal homepage: www.elsevier.com/locate/biochempharm

Convergence of ER stress and ferroptosis in diabetic vasculopathy: therapeutic protection by ferrostatin-1

Yue Ma [a,1], Junjia Gao [b,1], Yaqian Sun [a], Yufan Gu [a], Lu Zhang [a], Yanru Zhen [a], Hui Jia [c], Yueyang Liu [a,*], Qian Xu [a,*], Ming-Sheng Zhou [a,*]

[a] Shenyang Key Laboratory of Vascular Biology, Institute of Life Science, Shenyang Medical College, Shenyang 110034, China
[b] Department of Cardiology, The 2nd Affiliated Hospital of Shenyang Medical College, 110002, China
[c] School of Traditional Chinese Medicine, Shenyang Medical College, Shenyang 110034, China

ARTICLE INFO

Keywords:
Diabetic vasculopathy
Endoplasmic reticulum stress
Endothelial insulin resistance
Ferroptosis
Oxidative stress

ABSTRACT

Diabetic vascular complications are driven by endothelial dysfunction and insulin resistance, their underlying mechanisms remain incompletely understood. Ferroptosis, an iron-dependent form of regulated cell death characterized by lipid peroxidation, has been implicated in various diseases. However, its role in diabetic vasculopathy is unclear. This study investigated the contribution of ferroptosis to diabetic endothelial injury and its interplay with oxidative and endoplasmic reticulum (ER) stress. In diabetic *db/db* mice, the ferroptosis inhibitor ferrostatin-1 (Fer-1) reduced aortic thickness (−65%), reactive oxygen species production (−87.3%), and improved endothelium-dependent relaxation to acetylcholine (75.6%) and insulin (73.1%), independent of glycemic control. In human umbilical vein endothelial cells (HUVECs), high glucose induced ferroptosis, evidenced by mitochondrial shrinkage, downregulation of glutathione peroxidase 4/ solute carrier family 7 member 1 (SLC7A11), and lipid peroxidation. Fer-1 co-treatment suppressed these effects, concurrently alleviating oxidative/ER stress and restoring insulin-stimulated phosphoinositide 3-kinase/AKT/endothelial nitric oxide synthase signaling. Mechanistically, quenching oxidative stress with N-acetylcysteine attenuated high glucose-induced ER stress, ferroptosis, and insulin resistance. Furthermore, inhibiting ER stress or silencing the pro-apoptotic transcription factor C/EBP homologous protein (CHOP), a known repressor of SLC7A11, attenuated high glucose-induced ferroptosis and partially restored insulin signaling. Our findings suggest the presence of a pathway in which high glucose-driven oxidative stress may initiate ER stress, leading to CHOP-mediated suppression of SLC7A11 and subsequent ferroptosis, thereby contributing to endothelial insulin resistance. These results raise the possibility that targeting ferroptosis could represent a promising therapeutic strategy for diabetic vascular complications, possible through mechanisms distinct from glucose-lowering.

Abbreviations: ATF4, activating transcription factor 4; BCA, bicinchoninic acid; CCK-8, cell counting kit-8; CHOP, C/EBP homologous protein; DCFH-DA, 2′,7′-Dichlorodihydrofluorescein diacetate; DHE, dihydroethidium; DMSO, dimethyl sulfoxide; eIF2α, eukaryotic initiation factor 2α; eNOS, endothelial nitric oxide synthase; ER, endoplasmic reticulum; Fer-1, ferrostatin-1; FTH1, ferritin heavy chain 1; GPX4, glutathione peroxidase 4; GRP78, glucose-regulated protein 78; GSH, reduced glutathione; GSSG, oxidized glutathione disulfide; HBSS, hanks' balanced salt solution; HE, hematoxylin and eosin; HG, high glucose; HRP, horseradish peroxidase; HUVECs, human umbilical vein endothelial cells; HMEC-1, Human Microvascular Endothelial Cell line-1; 4HNE, 4 Hydroxynonenal; INS, insulin; ITT, Insulin tolerance test; NAC, N-acetylcysteine; NG, normal glucose; Nrf2, nuclear factor erythroid 2-related factor 2; OS, osmotic stress; PBS, phosphate-buffered saline; PERK, Protein kinase RNA-like endoplasmic reticulum kinase; PI3K, phosphatidylinositol 3-kinase; PSS, physiological salt solution; PVDF, polyvinylidene fluoride; ROS, reactive oxygen species; SBP, systolic blood pressure; SDS-PAGE, sodium dodecyl sulfate–polyacrylamide gels; siCHOP, siRNA targeting CHOP; siNC, non-targeting scrambled siRNA; SLC7A11, solute carrier family 7 member 11; siRNA, small interfering RNA; TC, total cholesterol; TEM, transmission electron microscopy; TBST, tris-buffered saline containing 0.1% Tween-20; TG, total triglyceride; T2DM, Type 2 diabetes mellitus; TFR, transferrin; TUDCA, tauroursodeoxycholic acid.

* Corresponding authors at: Shenyang Key Laboratory of Vascular Biology, Institute of Life Science, Huanghe N St. 146, Shenyang 110034, China.
E-mail addresses: liuyueyang@symc.edu.cn (Y. Liu), xuqiandoctor@symc.edu.cn (Q. Xu), zhoums@symc.edu.cn (M.-S. Zhou).
[1] Equally contribute to this work.

https://doi.org/10.1016/j.bcp.2026.117998
Received 27 November 2025; Received in revised form 13 April 2026; Accepted 17 April 2026
Available online 21 April 2026
0006-2952/© 2026 Published by Elsevier Inc.

1. Introduction

Type 2 diabetes mellitus (T2DM) poses a profound global health burden, primarily driven by its devastating vascular complications [1]. A key mediator of this pathophysiology is endothelial dysfunction, where impaired insulin signaling plays a central role [2]. The inability of insulin to stimulate vasorelaxation via the phosphatidylinositol 3-kinase (PI3K)/Protein Kinase B (PKB/AKT)/endothelial nitric oxide synthase (eNOS) pathway represents a critical feature of endothelial insulin resistance [3–5]. This dysfunction promotes a pro-inflammatory and pro-contractile state, leading to vascular dysfunction and injury [6]. Chronic hyperglycemia serves as the primary instigator of this damage [7], initiating a cascade of metabolic disturbances that directly impair endothelial function and insulin-mediated vasorelaxation, thereby accelerating diabetic vasculopathy [8–10].

It has been shown that hyperglycemia drives endothelial injury through the sustained activation of intracellular stress pathways. Among them primary ones are oxidative stress and endoplasmic reticulum (ER) stress, which impairs protein homeostasis [11–14]. These mechanisms are intimately linked and serve as key instigators of the inflammatory and dysfunctional endothelial phenotype [15], directly impairing the insulin PI3K/AKT/eNOS signaling cascade and thereby promoting vascular insulin resistance [16].

Sustained oxidative stress and ER stress in the endothelium may create an ideal substrate for ferroptosis, a novel iron-dependent cell death pathway driven by catastrophic lipid peroxidation [17,18]. The metabolic disturbances of diabetes, including glutathione depletion and altered iron homeostasis, can directly prime this process [19,20]. We propose that ferroptosis acts not as a parallel pathway, but as a critical convergent mechanism through which unresolved oxidative and ER stress ultimately execute cellular demise and exacerbate impairment of insulin signaling in the vasculature [21,22].

Although ferroptosis has been proposed as an important mechanism of diabetic endothelial injury, its regulatory pathways remain poorly defined [23]. ER stress can promote ferroptosis, a process in which the upregulation of the effector protein C/EBP homologous protein (CHOP) may play an important role by depleting glutathione and inhibiting the key antioxidant enzyme glutathione peroxidase (GPX) 4 [24–26]. Conversely, the lipid peroxidation and membrane damage caused by ferroptosis can impair ER function, creating a vicious cycle that amplifies both forms of cellular stress and leads to cell death [27]. A critical unanswered question is whether a causal link exists, whereby ER stress acts as an upstream activator of ferroptosis in the diabetic endothelium. This connection is plausible given their shared drivers including reactive oxygen species (ROS)and the capacity of the ER stress effector CHOP to repress antioxidant defense genes, thereby potentiating lipid peroxidation [27,28]. However, this potential convergence of ER stress and ferroptosis, and its specific role in disrupting vascular insulin signaling, has not been investigated, presenting a significant knowledge gap in our understanding of diabetic vasculopathy [29].

To investigate this potential mechanistic nexus and explore a novel therapeutic strategy, we employed the specific ferroptosis inhibitor ferrostatin-1 (Fer-1), a potent radical-trapping antioxidant [30]. We hypothesize that ER stress promotes ferroptosis, which constitutes a key mechanism disrupting insulin signaling in diabetic endothelium, and that inhibiting ferroptosis with Fer-1 will confer protection. To test this hypothesis, we utilized both an *in vivo* diabetic *db/db* mice and an *in vitro* model of high glucose-treated endothelial cells. We designed our investigation with three interconnected tiers: first, to determine whether Fer-1 treatment alleviates vascular injury, improves insulin-mediated vasorelaxation, and reduces oxidative stress markers in diabetic *db/db* mice; second, to investigate whether Fer-1 protects against high glucose-induced cytotoxicity, ROS, ER stress, ferroptosis, and impaired insulin AKT/eNOS signaling in endothelial cells; and third, to mechanistically probe the causal link from ER stress to ferroptosis utilizing antioxidants and ER stress inhibitors and genetic knockdown of the key effector CHOP via small interfering RNA (siRNA).

2. Methods

2.1. Animal grouping and experimental procedures

All animal procedures were conducted in compliance with the National Institutes of Health (NIH) guidelines for the Care and Use of Laboratory Animals and were approved by the Ethics Committee of Shenyang Medical College (Approval No: SYYXY20240202). Ten-week-old male *db/db* mice and control *db/m* littermates on a C57BL/6J background were obtained from the GemPharmatech Co., Ltd., (Nanjing, China). The animals were housed under specific pathogen-free conditions in the Laboratory Animal Center of Shenyang Medical College (Shenyang, Liaoning, China). After a two-week acclimatization period, the mice were randomly divided into three groups: Control group (Ctrl, n = 6): *db/m* littermates receiving an equal volume of solvent; Diabetic group (db/db, n = 6): *db/db* mice receiving an equal volume of solvent; Diabetic Fer-1 treatment group (db/db + Fer-1, n = 6): *db/db* mice treated with Fer-1. All mice were fed a standard mouse diet. Fer-1 was administered daily via intraperitoneal injection at a dose of 5 mg/kg for 8 weeks. Fer-1 was first dissolved in a vehicle consisting of 5% dimethyl sulfoxide (DMSO), 40% polyethylene glycol (PEG)300, 5% Tween 80 and 50% double-distilled water, then diluted to achieve a final DMSO concentration of less than 0.5%. Mice in the control and diabetic groups received intraperitoneal injections of an equivalent volume of solvent solution.

Body weight was measured weekly, and fasting blood glucose levels were assessed weekly using an automatic blood glucose monitoring system (Roche Accu-CHEK Active, Mannheim, Germany). One week prior to the end of the study, all mice underwent daily training for 5 consecutive days to acclimate to blood pressure measurements. Systolic blood pressure (SBP) was measured using a tail-cuff system (Softron Biotechnology Co., Ltd., Beijing, China) in conscious mice under quiet and dim lighting conditions, as previously described [31]. At least five consecutive readings were recorded, and the average value was calculated for each mouse. At the end of the experimental period, mice were fasted overnight and anesthetized with isoflurane (3% isoflurane, R510, RWD Life Technology Co., Ltd., Shenzhen, China). Blood samples were collected via left ventricular puncture. Plasma was used for measurement of total cholesterol (TC) and triglyceride (TG). Serum levels of total TC and TG were quantified using the assay kit (Nanjing Jiangchen Bioengineering Institute Co., Nanjing, China) according to the COD-PAP (A111-1-1) method and GPO-PAP (A110-1-1) enzymatic method, respectively. The aorta was carefully isolated and processed for subsequent organ chamber experiments or histological analysis.

2.2. Histological analysis

The thoracic aorta, harvested from a segment 1 cm below the apex of the aortic arch, was isolated and fixed in 4% paraformaldehyde prepared in phosphate-buffered saline (PBS). The fixed tissue samples were sectioned at a thickness of 4 μm and stained with hematoxylin and eosin (HE, Beyotime, Biotechnology, Jiangsu, C0105M). Sections were imaged using a Leica DM4B fluorescence microscope. For each animal, three non-consecutive sections were selected, and two images per section were acquired. The radial thickness of the media was measured using ImageJ software (version 1.48v). To evaluate aortic fibrosis, Masson's trichrome staining (Beyotime, Biotechnology, Jiangsu, C0189M) was performed. Semiquantitative analysis of fibrosis was carried out with ImageJ (version 1.48v), and the results were expressed as the percentage of positively stained area relative to the total area analyzed. All image acquisition and quantitation procedures were performed in a blinded manner, with evaluators having no knowledge of the experimental group assignments.

2.3. Organ chamber bath experiments

Endothelium-dependent relaxation to acetylcholine or insulin was performed as previously described [32]. Briefly, aortic rings were carefully cleaned of adherent connective tissue and sectioned into 3-mm segments. Each ring was mounted in a 4-channel tissue bath system (DMT Inc., Denmark) filled with oxygenated (95% O_2 and 5% CO_2) physiological salt solution (PSS) at 37°C. The rings were gradually stretched to an optimal resting tension of 1 g and allowed to equilibrate for 90 min. After equilibration, vessel was preconstructed by two successive exposures to PSS containing 60 mmol/L KCl. Rings that produced robust and reproducible contractions were used for further experiments. To evaluate endothelium-dependent relaxation, the rings were precontracted with norepinephrine (~30 nmol/L; Sigma-Aldrich, St. Louis, MO, USA) to approximately 70% of their maximal constriction. Cumulative concentration–response curves for acetylcholine (10^{-9} to 10^{-5} mol/L, Sigma-Aldrich, A2661) or insulin (10^{-9} to 10^{-6} mol/L, Sigma Aldrich, SLBZ8936) were then obtained. Relaxation responses to acetylcholine and insulin were expressed as the percentage inhibition of the precontraction induced by norepinephrine.

2.4. Determination of aortic ROS using dihydroethidium (DHE) fluorescence staining

ROS production was measured by DHE fluorescence staining, following a previously described method [32]. Paraffin-embedded aortic tissue sections were deparaffinized and rehydrated according to standard protocols. The sections were then incubated with 10 μmol/L DHE fluorescent probe (Beyotime, Biotechnology, Jiangsu, S0063), prepared in DMSO, at 37°C for 30 minutes in a light-protected environment to permit DHE oxidation by intracellular ROS. After incubation, the samples were rinsed with PBS and stored at 4°C. Fluorescence quantification was performed within 30 minutes. Images were acquired using an inverted fluorescence microscope with excitation at 488 nm and emission at 610 nm. Fluorescence intensity per unit area, indicative of ROS levels, was quantified using ImageJ software [33].

2.5. Cell culture

Human umbilical vein endothelial cells (HUVECs) were purchased from American Type Culture Collection Inco. (ATCC, Catalog #: CRL-2922, female origin, Manassas. Virginia), and human microvascular endothelial cell line-1 (HMEC-1) were obtained from Shanghai EK-Bioscience Biotechnology Co., Ltd. (Shanghai, China). Both HUVECs and HMEC-1 were maintained with glucose–free Dulbecco's Modified Eagle Medium (DMEM, Pricella, PM150322, Wuhan Pricella Biotechnology Co., Ltd., Wuhan, China) supplemented with 10% fetal bovine serum, 1% penicillin/streptomycin, and exogenous glucose to a final concentration of 5.5 mmol/L, and maintained at 37 °C in a 5% CO_2 atmosphere prior to experimental treatments. Cells were seeded in 6-well plates (3.0×10^5 cells/well). For HUVEC experiment, cells were divided into four primary groups: a normoglycemic control (5.5 mmol/L glucose), a normoglycemic control treated with Fer-1 (10 μmol/L, Selleck, Houston, TX, S7243), a hyperglycemic group (30 mmol/L glucose), and a hyperglycemic group treated with Fer-1. Fer-1 was dissolved in DMSO, and control groups received an equivalent volume of the DMSO vehicle. In a subset of experiments, Fer-1 was substituted with the antioxidant N-acetylcysteine (NAC, 1 mmol/L; Beyotime, Biotechnology, Nanjing, China, S0077) or ER stress inhibitor tauroursodeoxycholic acid (TUDCA, 100 μmol/L, Selleck, Houston, TX, S3654). To assess the insulin signaling pathway, cells were stimulated with 100 nmol/L insulin for 15 minutes prior to harvest following the respective treatments.

Additional experiments were performed in HMEC-1 to exclude potential osmotic effects of high glucose. Cells were treated with normal glucose (NG, 5.5 mmol/L), high glucose (HG, 30 mmol/L), or osmotic control medium containing 5.5 mmol/L glucose plus 24.5 mmol/L mannitol, in the presence or absence of Fer-1. Cell viability, intracellular ROS production, ER stress markers, and some ferroptosis-related protein expressions were subsequently assessed using the same experimental procedures as described for HUVECs.

2.6. siRNA transfection

Gene silencing of CHOP was performed using siRNA. HUVECs were transfected with 50 nmol/L of CHOP-targeting siRNA (siCHOP). A non-targeting scrambled siRNA sequence (siNC) was used as a negative control in all experiments. All siRNA molecules were synthesized by RiboBio Co., Ltd. (Guangzhou, China). Transfection was carried out according to the manufacturer's instructions using a standard lipid-based transfection reagent.

Following transfection, cells were allocated into four groups: (1) normoglycemic siNC control, (2) normoglycemic siCHOP, (3) hyperglycemic siNC, and (4) hyperglycemic siCHOP. The hyperglycemic condition was established by culturing cells in medium containing 30 mmol/L glucose, while the normoglycemic control contained 5.5 mmol/L glucose. Cells were subjected to their respective treatments for a predetermined period post-transfection before harvest. The efficiency of CHOP knockdown was confirmed by Western blot analysis prior to subsequent experiments.

To further investigate the role of CHOP in regulating intracellular redox homeostasis, the ratio of reduced glutathione (GSH) to oxidized glutathione (GSSG) (GSH/GSSG) was measured in siRNA-transfected cells using a commercial GSH and GSSG Assay Kit (Beyotime Biotechnology, Jiangsu, S0053) according to the manufacturer's instructions. Experimental grouping for the GSH/GSSG assay was identical to that described above.

2.7. CCK-8 assay

Cell viability was assessed using a cell counting kit-8 (CCK-8; Vazyme, Nanjing, China, A311-02) according to the manufacturer's instructions. HUVECs or HMEC-1 cells were seeded into 96-well plates at a density of 2×10^4 cells per well and allowed to adhere overnight.

For HUVEC experiments, cells were treated for 24 or 48 hours under the following conditions: NG (5.5 mmol/L), HG (30 mmol/L), high glucose plus the antioxidant NAC, or high glucose plus Fer-1. In a separate experiment, CHOP expression was silenced by transfecting HUVECs with siCHOP, using siNC as a negative control.

To further validate the effects of hyperglycemia and ferroptosis in microvascular endothelial cells, additional experiments were performed in HMEC-1. For dose-response studies, cells were exposed to increasing glucose concentrations (5.5, 10, 20, and 30 mmol/L) for 24 hours. For time-course analysis, HMEC-1 cells were treated with high glucose (30 mmol/L) for different durations (0, 24, and 48 hours). To determine the involvement of different cell death pathways, HMEC-1 cells were treated with high glucose in the presence or absence of specific cell death inhibitors, including Fer-1 (ferroptosis inhibitor, 10 μmol/L, MedChemExpress, Monmouth Junction, NJ, USA, HY-100579), Z-VAD-FMK (HY-16658B, pan-caspase inhibitor, apoptosis inhibitor, 100 μmol/L, MedChemExpress), Necrostatin-1 (HY-15760, necroptosis inhibitor, 50 μmol/L, MedChemExpress). MCC950 (HY-12815, pyroptosis inhibitor, 10 μmol/L, MedChemExpress).

After the designated treatment period, 10 μL of CCK-8 solution was added to each well, and the plates were incubated at 37°C for 2 hours. Absorbance was measured at 450 nm using a microplate reader (BGM LABTECH, Ortenberg, Germany). All samples were analyzed in technical duplicate across three biological replicates.

2.8. Transmission electron microscopy (TEM)

HUVECs were fixed with 2.5% glutaraldehyde in PBS at 4°C and

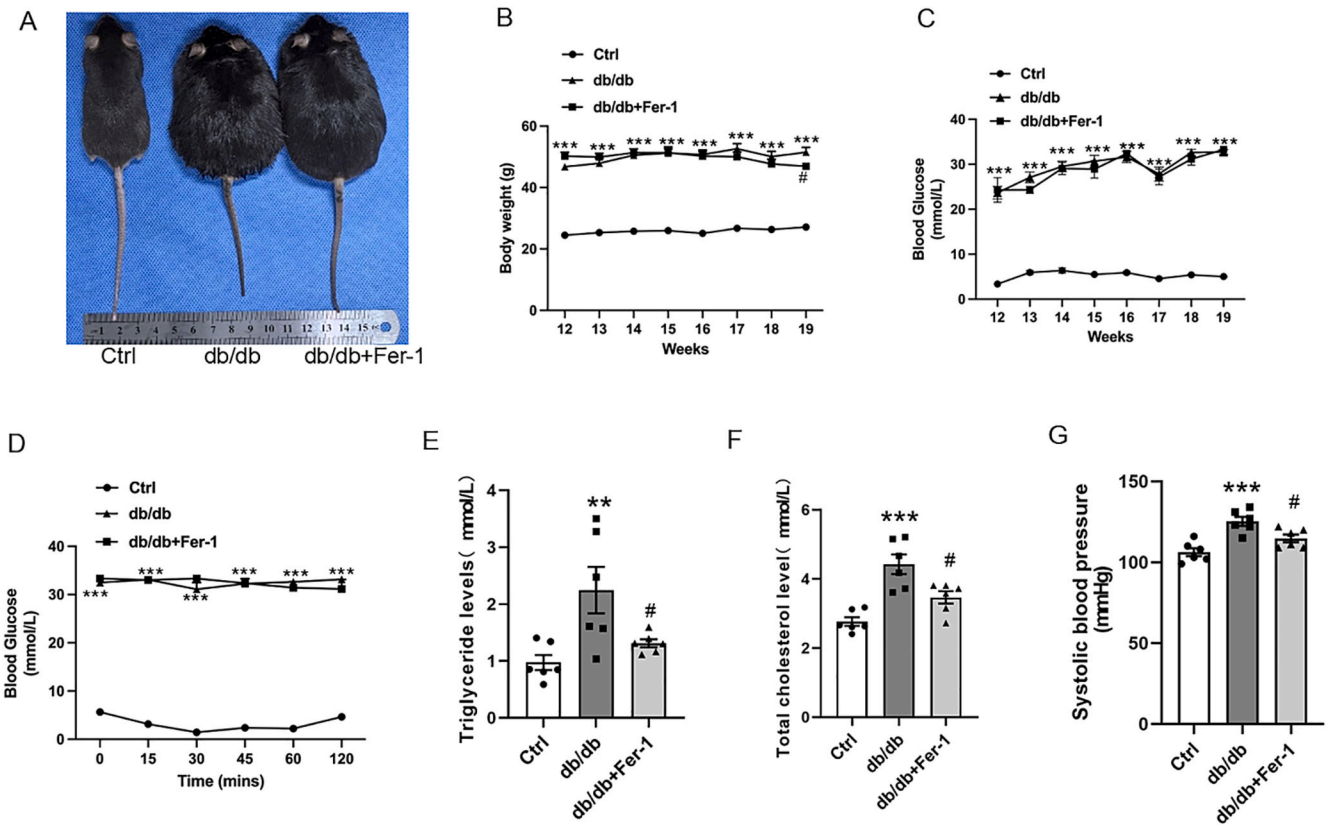


Fig. 1. Ferrostatin 1 (Fer-1) improves metabolic parameters in diabetic db/db mice independent of glycemic control. (A) Comparative gross appearance of mice and (B) body weight; (C) Fasting blood glucose; (D) Insulin tolerance test (ITT); (E) Total serum triglyceride (TG); (F) Total serum total cholesterol (TC) and (G) Systolic blood pressure (SBP). N = 6. Data are presented as mean ± SEM. ***p<0.001, **p<0.01, vs. control (Ctrl) group; #p<0.05 vs. db/db group.

subsequently post-fixed with 1% osmium tetroxide. The samples were then dehydrated through a graded series of ethanol solutions and embedded in epoxy resin. Following polymerization, ultra-thin sections (approximately 90 nm thick) were cut and mounted on uncoated copper grids. The sections were contrast-stained with 2% uranyl acetate followed by Reynolds' lead citrate (0.1%). Finally, the prepared grids were examined and imaged using a HITACHI H-7650 TEM operating at an acceleration voltage of 80 kV (FEI Tecnai, G2 120KV, USA).

2.9. Measurement of intracellular ferrous iron (Fe^{2+}) with FerroOrange staining

To quantify the intracellular Fe^{2+} level, HUVECs were subjected to FerroOrange fluorescence staining. The cells were loaded with 1 μmol/L FerroOrange (Dojindo Molecular Technologies, Kumamoto, Japan, F374) in Hanks' Balanced Salt Solution and incubated at 37°C for 30 minutes in the dark to allow the dye to penetrate and chelate intracellular Fe^{2+}. After the incubation period, fluorescent images were acquired using a fluorescence microscope. For quantification, the average fluorescence intensity was calculated from the images using ImageJ software. This was done by measuring the integrated density (total fluorescence intensity) within the cell boundaries, normalizing it to the total cellular area, and subtracting the background signal from a cell-free region. Final concentrations are expressed as mean fluorescence density.

2.10. Determination of intracellular ROS using flow cytometry

To assess intracellular ROS levels, HUVECs were incubated with normal or high glucose with or without Fer-1 treatment for 24 hours. Then cells were incubated with 10 μmol/L 2′,7′-Dichlorodihydrofluorescein diacetate (DCFH-DA, Beyotime Biotechnology, Nanjing, China, S0033S) in serum-free medium at 37°C for 30 minutes in the dark. This cell-permeable probe is deacetylated by intracellular esterases to non-fluorescent compound DCFH, which is subsequently oxidized to highly fluorescent DCF in the presence of ROS. Following incubation, the cells were washed twice with PBS to remove residual probe. The fluorescence intensity of DCF, proportional to ROS levels, was immediately analyzed using a flow cytometer (NovoCyteAdvanteon, Agilent Biotechnology Co., Ltd., Santa Clara, USA). For each sample, a total of 100,000 events were recorded, and the DCF-DA positive ratio was quantified, and relative fluorescence intensity was normalized to the normoglycemia group.

2.11. Western blot analysis

Protein lysates were prepared from HUVECs, HMEC-1 or homogenized aortic tissues using RIPA lysis buffer supplemented with protease and phosphatase inhibitors. Protein concentration was determined with a bicinchoninic acid (BCA)protein assay kit (Beyotime Biotechnology, Nanjing, China, P0010) according to the manufacturer's instructions. Equal amounts of protein (50 μg per lane) were separated by electrophoresis on 8–12% sodium dodecyl sulfate-polyacrylamide gels and subsequently transferred onto polyvinylidene fluoride membranes. The membranes were blocked for 1 hour at room temperature with 5% non-fat milk in Tris-buffered saline containing 0.1% Tween-20 (TBST). Following blocking, membranes were incubated overnight at 4°C with specific primary antibodies diluted in blocking buffer. The primary antibodies were as follows: anti-glucose-regulated protein 78 (GRP78; Proteintech, Rosemont, USA, 11587-1-AP); anti-CHOP (Proteintech, 15204-1-AP), anti-solute carrier family 7 member 11 (SLC7A11; ABclonal, Wuhan, China, A13685), anti-GPX4 (Abcam, Cambridge, UK,

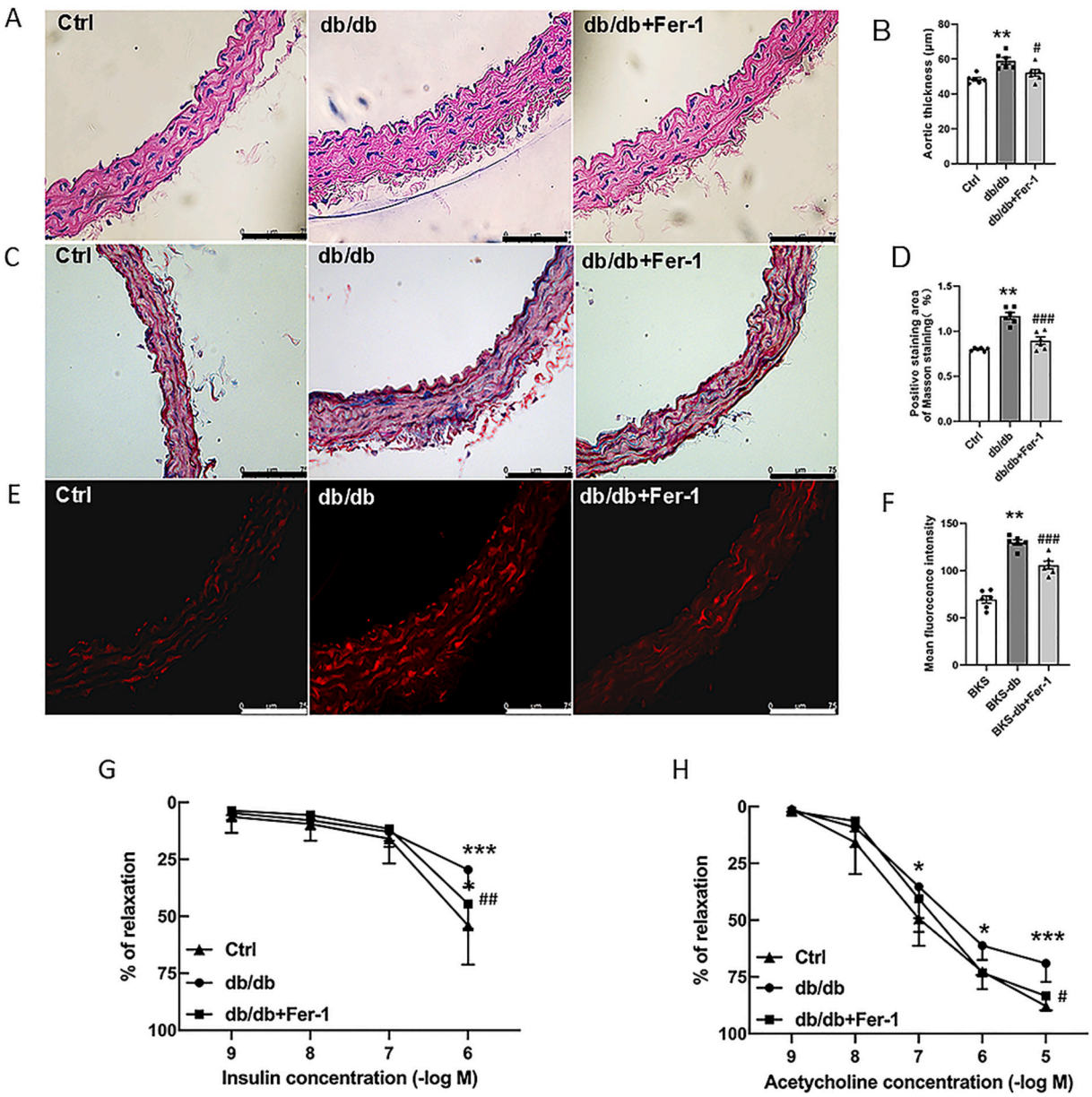


Fig. 2. Fer-1 ameliorates aortic remodeling, oxidative stress, and endothelium-dependent relaxation to acetylcholine and insulin in *db/db* mice. Representative images (A) and quantification (B) of aortic section by Hematoxylin & Eosin (HE) staining; Representative images (C) and semiquantitative analysis (D) of aortic section by Masson's trichrome staining. (E) Representative dihydroethidium (DHE) fluorescence staining of aortic reactive oxygen species (ROS) and its quantification analysis (F). Acetylcholine- (G) or insulin- (H) induced endothelium-dependent vasorelaxation in aortic rings. N = 6. ***p<0.001, **p<0.01, *p<0.05 vs. Ctrl group; ###p<0.001, ##p<0.01, #p<0.05 vs. db/db group. Scale bar: 75 μm.

AB125066), anti-ferritin heavy chain 1 (FTH1, ABclonal, 4393), anti-transferrin (TFR, Abcam, AB214039), anti-nuclear factor erythroid 2-related factor 2 (Nrf2, Abmart, Berkeley Heights, NJ, USA, T55136M); anti-AKT (Abmart, T55561F), anti-P-AKT Ser473 (Abmart, T40067S), anti-4 Hydroxynonenal (4HNE, Abcam, AB46545), and anti-eNOS (ABclonal, A20985), anti-P-eNOS Ser1177 (ABclonal, AP0515).

After incubation with primary antibodies, membranes were washed with TBST and then incubated for 1 hour at room temperature with appropriate horseradish peroxidase-conjugated secondary antibodies: goat anti-mouse IgG. Protein bands were visualized using a Bio-Rad chemiluminescence detection system. To ensure equal protein loading, membranes were stripped and re-probed with an anti- glyceraldehyde-3-phosphate dehydrogenase (GAPDH) antibody. Band intensities were quantified using ImageJ software. Data were normalized to GAPDH or to the corresponding total protein for phosphoproteins, and are expressed as a fold change compared to the control group.

To detect the Nrf2 protein expression in nuclear fraction, nuclear and cytoplasmic fractions were prepared from HMEC-1 using the NE-PER Nuclear and Cytoplasmic Extraction Kit (Beyotime Biotechnology, Nanjing, China, P0028) according to the manufacturer's instructions. Briefly, cells were harvested, gently lysed in cytoplasmic extraction buffer, and centrifuged at 16,000 × *g* for 5 minutes. The insoluble pellet containing nuclei was resuspended in nuclear extraction buffer, incubated on ice for 30 minutes with vortexing every 10 minutes, and centrifuged at 16,000 × *g* for 10 minutes. The supernatant (nuclear fraction) was collected to detect nuclear Nrf2 expression using Western blot analysis. Data were normalized to LaminA/C, and are expressed as a fold change compared to the control group.

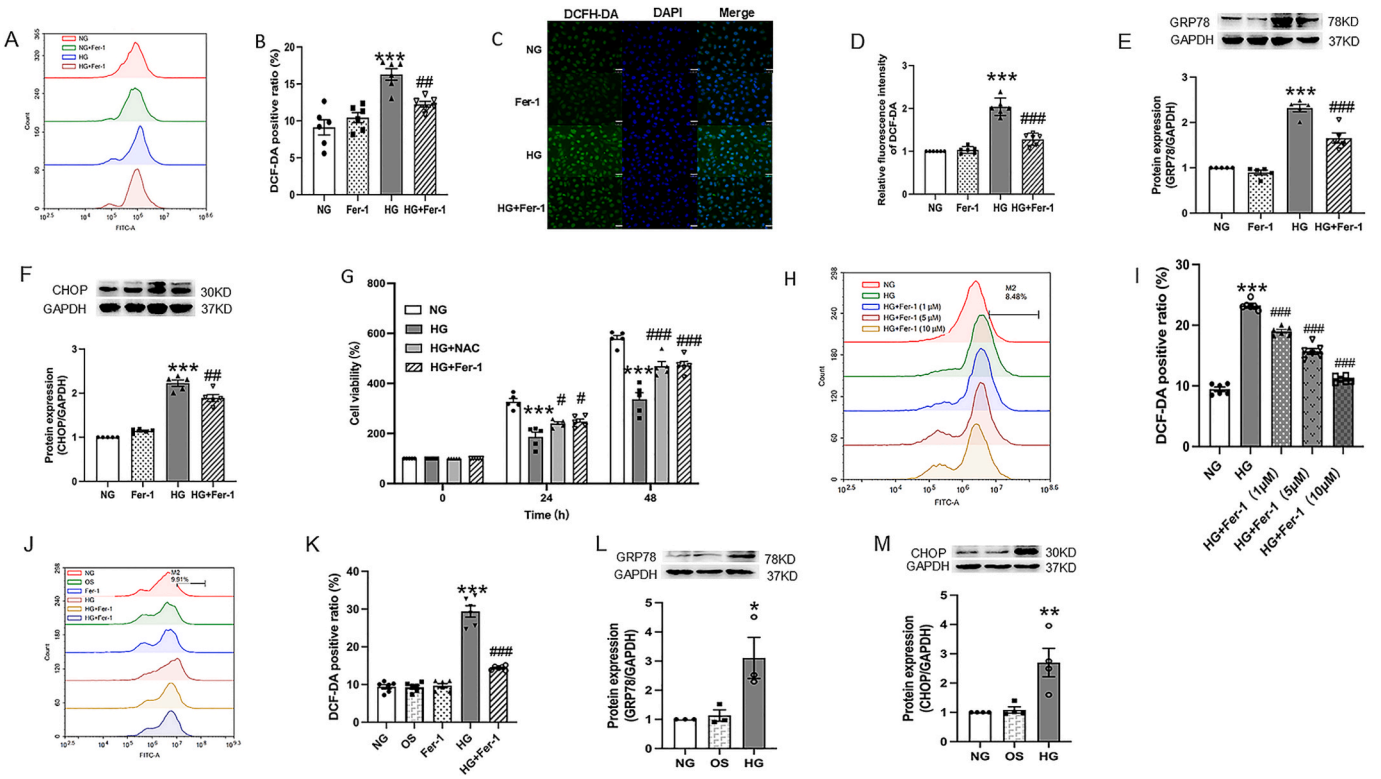


Fig. 3. Fer-1 mitigates high glucose-induced ROS, endoplasmic reticulum (ER) stress, and loss of cell viability in human umbilical vein endothelial cells (HUVECs, A-G) and human microvascular endothelial cell line-1 (HMEC-1, H-M). (A) Representative flow cytometry histograms and (B) quantification of intracellular ROS in HUVECs, N = 6; (C) Representative images and (D) quantification of oxidative fluorescence in HUVECs stained with 2',7'-Dichlorodihydrofluorescein diacetate (DCFH-DA), N = 6; (E-F) Western blot analysis and quantification of ER stress markers (E) glucose-regulated protein (GRP)78, N = 5 and (F) C/EBP homologous protein (CHOP), N = 5; (G) Cell viability in HUVECs; (H-K) Effect of Fer-1 on ROS production in HMEC-1, determined by flowcytometry, N = 6; (L-M): Osmotic stress did not affect protein expression of GRP78, N = 3 (L) and CHOP, N = 4 (M) in HMEC-1. ***p<0.001, **p<0.01, *p<0.05 vs. NG group; ###p<0.001, ##p<0.01, #p<0.05 vs. high glucose (HG) group. Scale bar: 25 μm.

2.12. Statistical analysis

Data are presented as the mean ± standard error of the mean (SEM). All statistical analyses were performed using GraphPad Prism software (version 8.0 or higher). The exact number of independent replicates (n) is provided in each figure legend, where 'n' represents the number of independent biological replicates. Technical replicates were averaged for each biological replicate prior to statistical analysis. For comparisons involving more than two groups, one-way or two-way analysis (concentration-response curves) of variance (ANOVA) was performed as appropriate, followed by Tukey's post hoc test for multiple comparisons.

The sample size for *in vivo* experiments (n = 6 per group) was determined based on an a priori power analysis, anticipating a large effect size (Cohen's $f \geq 0.40$) for primary endpoints based on preliminary data and previous literature. This sample size was calculated to achieve at least 80% statistical power ($\alpha = 0.05$). A result was considered statistically significant when the p-value was less than 0.05 ($p < 0.05$).

3. Results

3.1. Fer-1 treatment improves metabolic parameters independent of glucose metabolism in db/db mice

As illustrated in Fig. 1, diabetic *db/db* mice displayed significant elevations in body weight, fasting blood glucose, serum TC and TG, accompanied by impaired glucose tolerance and a mild increase in SBP relative to non-diabetic controls. Eight-week treatment with Fer-1 elicited modest but significant reductions in body weight, total cholesterol, triglycerides, and SBP in *db/db* mice. Despite these effects, Fer-1 administration did not mitigate hyperglycemia or improve glucose tolerance. These results demonstrate that inhibition of ferroptosis ameliorates specific metabolic and hypertensive parameters in a manner largely independent of systemic glucose regulation.

3.2. Fer-1 alleviates aortic remodeling, oxidative stress, and endothelium-dependent relaxation to acetylcholine and insulin in db/db mice

Histological analysis revealed a significant increase in aortic wall thickness and fibrosis in *db/db* mice, as demonstrated by HE and Masson's trichrome staining, respectively; these structural abnormalities were attenuated by Fer-1 treatment (Fig. 2 A-D). Consistent with these findings, aortic oxidative stress, indicated by DHE fluorescence staining, was markedly elevated in *db/db* mice and subsequently reduced by Fer-1 (Fig. 2E, F). Functionally, the impaired endothelium-dependent relaxation in response to both acetylcholine and insulin observed in *db/db* mice was also ameliorated by Fer-1 treatment (Fig. 2 G and H).

3.3. Fer-1 mitigates oxidative stress and ER stress and improves cell viability in high glucose-treated endothelial cells

It has been shown that Fer-1 exerts protective effects through directly targeting the core ferroptosis pathway and indirectly mitigating associated oxidative and ER stress [34]. To investigate cellular mechanisms underlying Fer-1-mediated vascular protection, HUVECs derived from female donor were exposed to high glucose with or without ferroptosis inhibitor Fer-1. High glucose significantly increased ROS production, as measured by DCFH-DA fluorescence and flow cytometry, and this increase was inhibited by Fer-1 (Fig. 3 A-D). Furthermore, high glucose-

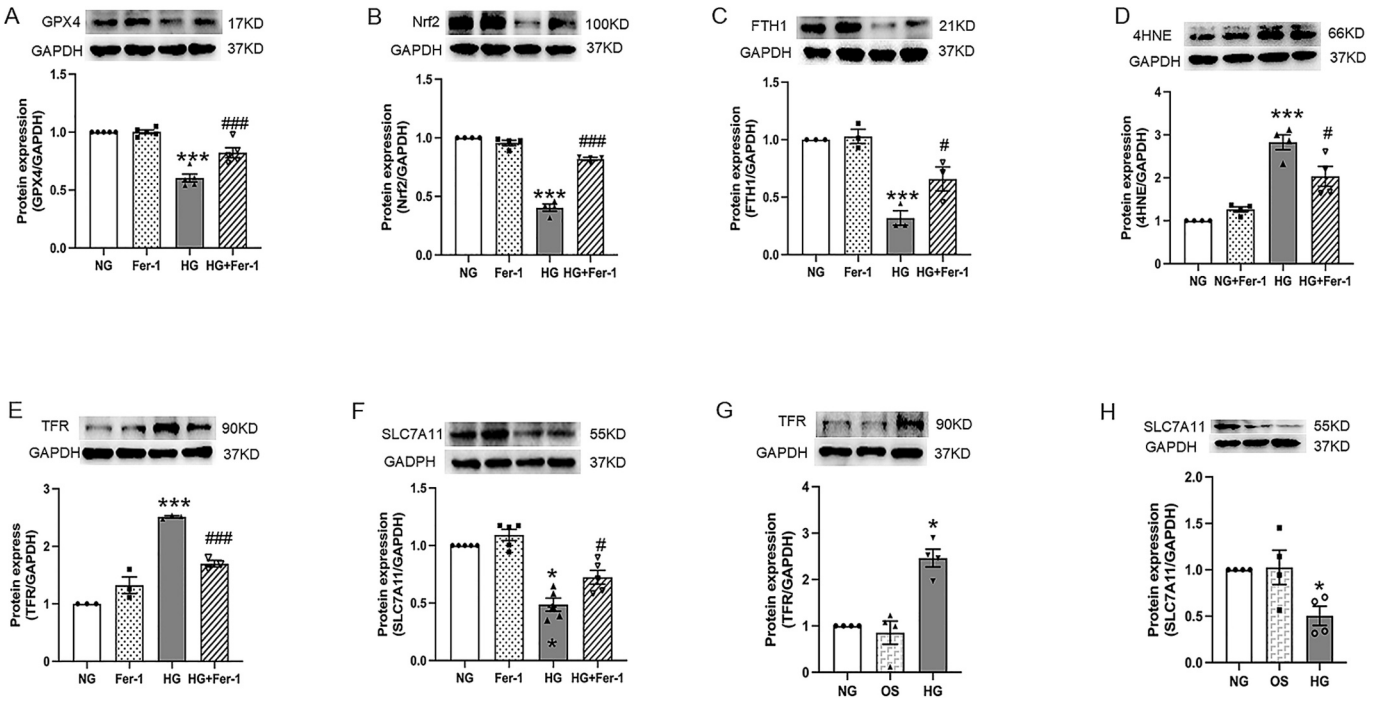


Fig. 4. Fer-1 counteracts high glucose-induced alterations in ferroptosis-related protein expression in endothelial cells. (A-F) Protein expression of key ferroptosis pathway proteins in HUVECs: (A) Glutathione peroxidase (GPX4), N = 5; (B) Nuclear factor erythroid 2-related factor (Nrf)2, N = 4; (C) Ferritin heavy chain (FTH)1, N = 3; (D) 4 -Hydroxynonenal (HNE), N = 4, (E) Transferrin receptor (TFR), N = 3; (F) Solute carrier family 7 member 11 (SLC7A11). (G-H) Osmotic stress did not affect the protein expression of TFR (G) and SLC7A11 (H) in HMEC-1. N = 4, ***p<0.001, *p<0.05 vs. normal glucose (NG) group; ###p<0.001, #p<0.05 vs. HG group.

induced upregulation of the ER stress markers GRP78 and CHOP was also attenuated by Fer-1 treatment (Fig. 3 E and F). This reduction in cellular stress was associated with a partial but significant improvement in high glucose-impaired cell viability, as shown by CCK-8 assay (Fig. 3 G).

To further validate glucose specificity and improve physiological relevance, additional experiments were performed using adult-derived HMEC-1. Using flow cytometry with DCFH-DA fluorescence, we found that Fer-1 reduced high glucose-induced ROS generation in a dose-dependent manner, with significant effects observed at 1 μmol/L and progressively greater inhibition at 5 μmol/L and 10 μmol/L (Fig. 3 H and I). Osmotic stress (OS) treatment did not significantly affect ROS production (Fig. 3 J and K), OS also did not affect ER stress markers glucose-regulated protein (GRP)78 and CHOP (Fig. 3 L and M), compared with normal glucose conditions, whereas high glucose induced similar alterations to those observed in HUVECs, including increased CHOP and GRP78 expression, confirming that the observed cellular injury was glucose-specific rather than due to hyperosmolarity.

3.4. Fer-1 inhibits high glucose-induced ferroptosis and restores insulin activation of the PI3K/eNOS pathway in endothelial cells

To investigate the mechanism by which Fer-1 inhibits high glucose-induced ferroptosis, we analyzed key markers of the ferroptosis pathway in HUVECs. High glucose treatment significantly downregulated the expression of antioxidant proteins GPX4 and Nrf2, as well as the iron storage protein ferritin heavy chain (FTH)1 (Fig. 4 A-C). Conversely, it upregulated the lipid peroxidation marker 4HNE and the iron import protein TFR (Fig. 4 D and E). Furthermore, given that the cystine/glutamate antiporter SLC7A11 is a critical gatekeeper of ferroptosis, we assessed its expression and found that high glucose significantly decreased SLC7A11, an effect partially reversed by Fer-1 co-treatment (Fig. 4 F). To rule out the influence of hyperosmolarity induced by high glucose, we treated HMEC-1 with osmotic control medium (mannitol, OS) and found that OS did not affect the expression of TFR and SLC7A11 (Fig. 4 G and H).

Furthermore, FerroOrange fluorescence staining revealed that Fer-1 attenuated the high glucose-induced accumulation of intracellular Fe^{2+} in HUVECs (Fig. 5 A and B).

Because Nrf2 activity depends on nuclear translocation, we further assessed nuclear Nrf2 levels. High glucose significantly reduced nuclear Nrf2 accumulation, whereas Fer-1 partially restored nuclear Nrf2 expression (Fig. 5 C), indicating improved Nrf2 activation. To further evaluate the functional status of the antioxidant system, intracellular glutathione balance was assessed. High glucose significantly reduced the GSH/GSSG ratio, while Fer-1 treatment partially restored glutathione homeostasis (Fig. 5 D), supporting preservation of the system Xc^{-}-GSH-GPX4 axis.

TEM analysis of mitochondrial morphology, a key hallmark of ferroptosis, demonstrated that high glucose caused characteristic mitochondrial morphological changes associated with ferroptosis, including mitochondrial shrinkage/swelling, loss of cristae, and an increased in dense particles, which were substantially reversed by Fer-1 (Fig. 5 E).

Given that impairment of the endothelial insulin pathway is a key mechanism in diabetic vasculopathy [35], we next examined the effect of Fer-1 on the phosphorylated AKT/eNOS signaling pathway. As expected, high glucose significantly impaired insulin-induced P-AKT (ser473) and P-eNOS (ser1177), and this impairment was reversed by Fer-1 treatment (Fig. 5 F and G). Interestingly, we also observed that high glucose significantly reduced basal phosphorylation levels of AKT (ser 473) and eNOS (ser1177) in HMEC-1 cells, and OS did not affect basal phosphorylation of AKT or eNOS (Fig. 5 H and I). Collectively, these results demonstrate that Fer-1 alleviates diabetic vasculopathy by inhibiting ER stress-induced ferroptosis, thereby restoring endothelial insulin signaling.

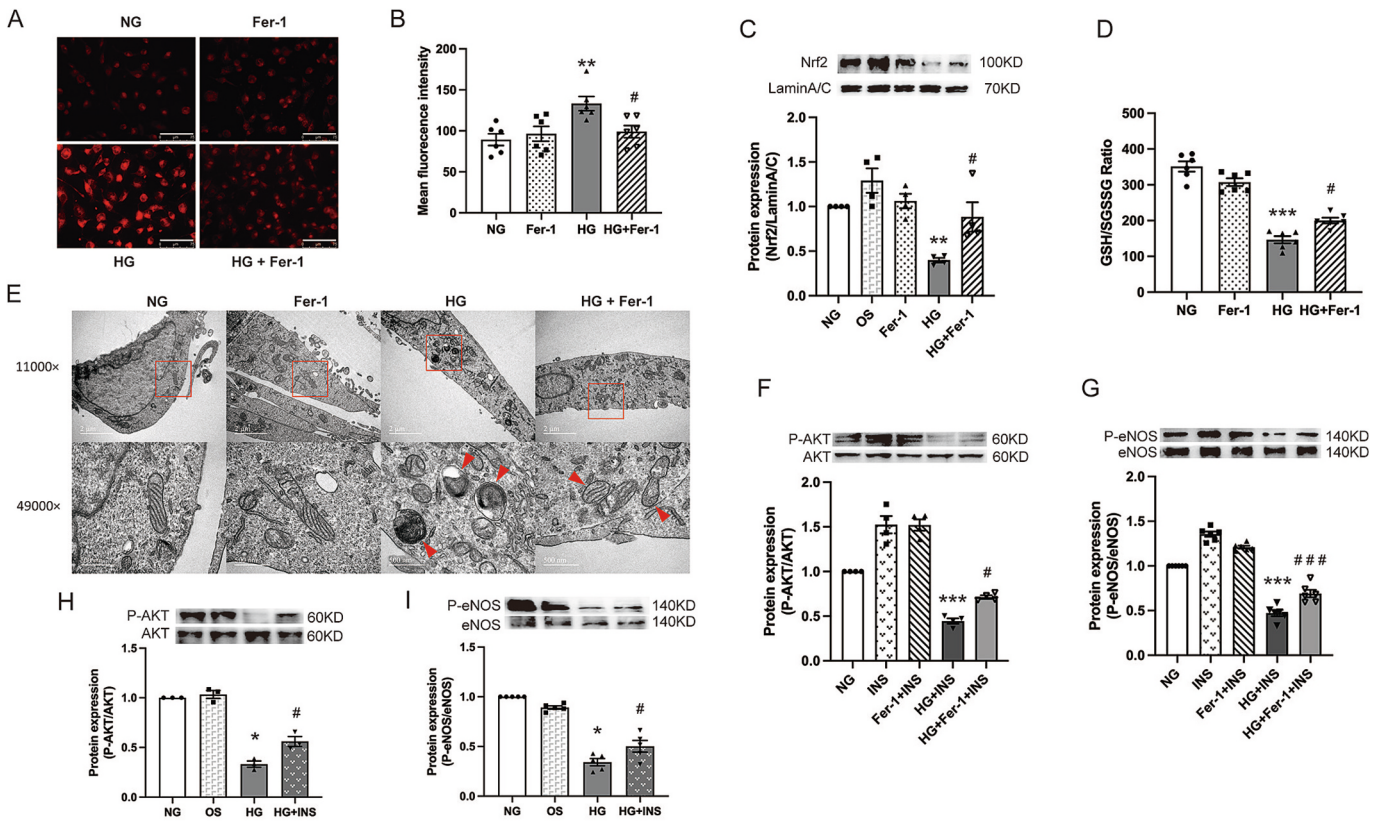


Fig. 5. Fer-1 inhibits high glucose-induced intracellular Fe^{2+} accumulation, mitochondrial damage, and restores insulin signaling in HUVECs (A-G) and HMEC-1(H-I). (A) Representative FerroOrange fluorescence images (scale bar: 75 μm), N = 6; (B) Quantification of FerroOrange fluorescence intensity. *p<0.05 vs. NG, N = 6; (C) Protein expression of Nrf2, N = 4; (D) Cellular GSH/GSSG ratio, N = 6; (E) Representative transmission electron microscopy (TEM) images of mitochondrial ultrastructure (scale bar: 2 μm or 500 nm). Red arrows indicate damaged mitochondria, N = 5; (F-G) Protein expression of P-AKT Ser473 (F) N = 4; and P-endothelial nitric oxidase synthase (P-eNOS) Ser1177 (G), N = 6. (H-I): Protein expression of P-AKT (Ser 473, H), N = 3 and P- eNOS, (ser1177, I), N = 5. ***p<0.001, **p<0.01, *p<0.05 vs. NG group or INS group; ###p<0.001, #p<0.05 vs. HG group or HG+INS group.

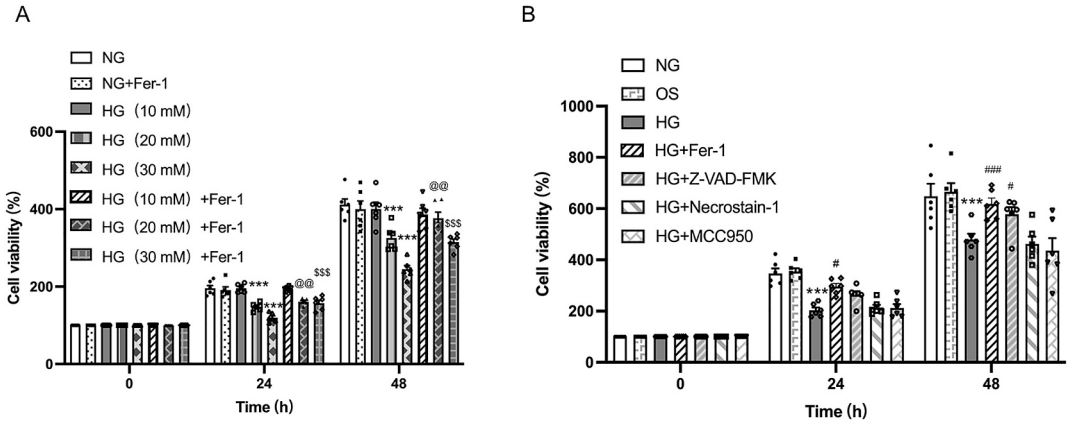


Fig. 6. Effects of different cell death inhibitors on cell viability under high glucose stress inHMEC-1. (A) Effects of different glucose concentration on cell viability at indicated time points (0, 24, 48 hours); (B) Effects of different cell death inhibitors on cell viability at indicated time points. Fer-1: ferroptosis inhibitor Fer-1. Z-VAD-FMK: apoptosis inhibitor; Necrostain-1: necrosis inhibitor; MCC950: pyroptosis inhibitor. N = 6, ***p<0.001 vs. NG group; @@p<0.01 vs. HG (20 mmol/L) group; $$$p<0.001 vs. HG (30 mmol/L) group; ###p<0.001, #p<0.05 vs. HG group.

3.5. Ferroptosis contributes to high glucose-induced endothelial injury alongside apoptosis but not necroptosis or pyroptosis

To determine the specificity of ferroptosis in high glucose-induced endothelial injury, HMEC-1 cells were treated with inhibitors targeting different programmed cell death pathways. High glucose but not mannitol significantly reduced cell viability in a time-dependent manner. Notably, this effect was also glucose concentration-dependent: compared to normal glucose (5.5 mmol/L), 10 mmol/L glucose did not affect cell viability, but further increasing glucose concentrations (20 mmol/L and 30 mmol/L) dose-dependently reduced viability, an effect partially reversed by Fer-1 treatment. Co-treatment with Fer-1 also significantly improved cell viability at both 24 hours (62.6%) and 48 hours (41.9) (Fig. 6 A). The apoptosis inhibitor z-VAD-

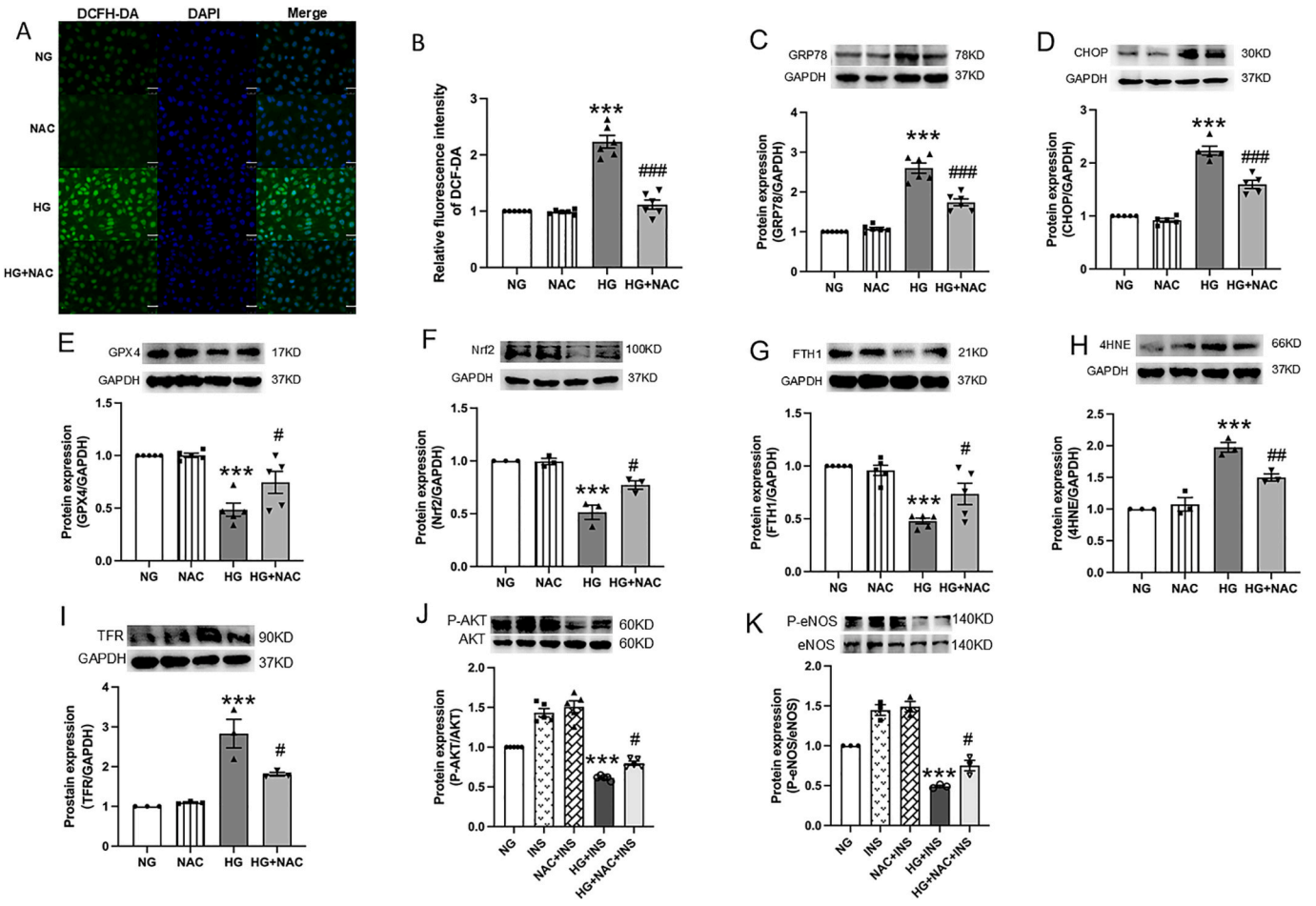


Fig. 7. The antioxidant N-acetylcysteine (NAC) attenuates high glucose-induced oxidative stress, ER stress, ferroptosis, and insulin signaling impairment in HUVECs. (A-B) Representative images (A) and quantification (B) of oxidative fluorescence stained with DCFH-DA (scale bar: 25 μm), N = 6; (C-D) Protein expression of ER stress markers GRP78, N = 6 and CHOP, N = 5; (E-I) Protein expression of ferroptosis-related proteins: (E) GPX4, N = 5; (F) Nrf2, N = 3; (G) FTH1, N = 5; (H) 4HNE, N = 3 (I) TFR, N = 3. (J) P-AKT Ser473, N = 5 and (K) P-eNOS Ser1177, N = 3. ***p<0.001 vs. NG group or INS group; ###p<0.001, ##p<0.01, #p<0.05 vs. HG group or HG+INS group.

fmk also partially rescued cell viability (58.5%), although the protective effect was weaker than that of Fer-1 at 48 hours (82.3%). In contrast, neither the necroptosis inhibitor necrostatin-1 nor the pyroptosis inhibitor MCC950 significantly affected cell viability (Fig. 6 B).

These results suggest that both ferroptosis and apoptosis contribute to high glucose-induced endothelial injury, whereas necroptosis and pyroptosis play minimal roles under these conditions.

3.6. NAC attenuates high glucose-induced oxidative stress, ER stress, ferroptosis, and insulin signaling impairment in HUVECs

Given the interconnected relationship between oxidative stress, ER stress, and ferroptosis [36], we investigated whether oxidative stress is an upstream driver of this deleterious cascade under high glucose conditions. To this end, we examined the effects of the antioxidant NAC. As expected, NAC treatment significantly attenuated high glucose-induced ROS production, as measured by DCFH-DA fluorescence (Fig. 7 A and B). This reduction was accompanied by decreased ER stress markers GRP78 and CHOP (Fig. 7 C and D). Concurrently, NAC restored the expression of GPX4, Nrf2, and FTH1 (Fig. 7 E-G), and reduced the levels of 4HNE and TFR (Fig. 7 H and I). Importantly, NAC also restored the insulin-stimulated phosphorylation of AKT Ser473 and eNOS Ser1177 impaired by high glucose (Fig. 7 J and K). These results support that oxidative stress is a critical upstream mediator linking high glucose to ER stress, ferroptosis and endothelial insulin signaling.

3.7. Inhibition of ER stress or CHOP silencing attenuates ferroptosis and restores insulin signaling in HUVECs

To investigate the role of downstream ER stress in high glucose-induced ferroptosis and impaired insulin signaling, endothelial cells were treated with the ER stress inhibitor TUDCA. TUDCA significantly attenuated the high glucose-induced upregulation of CHOP and concurrently reversed the downregulation of the key ferroptotic proteins GPX4 and SLC7A11 (Fig. 8A-C), and reversed the high glucose-induced impairment of insulin-stimulated AKT (Ser473) and eNOS (Ser1177) phosphorylation (Fig. 8 D and E), indicating improved insulin signaling.

Since CHOP is a known repressor of the System Xc^--GSH-GPX4 axis, we next examined its role using siRNA-mediated knockdown, CHOP expression was reduced by approximately 70% following siRNA transfection (Fig. 9 A). CHOP silencing effectively restored SLC7A11 and GPX4 levels under high glucose conditions (Fig. 9 B and C), increased cell viability (Fig. 9 D), and rescued the high glucose-induced impairment of insulin-stimulated AKT Ser473and eNOS Ser1177 phosphorylation (Fig. 9 E and F). Furthermore, CHOP knockdown significantly improved intracellular glutathione balance, as reflected by restoration of the GSH/GSSG ratio (Fig. 9 G), indicating preservation of the antioxidant defense system. Collectively, these results demonstrate that ER stress, acting through CHOP is a critical mediator linking high glucose exposure to ferroptosis activation and endothelial insulin signaling impairment.

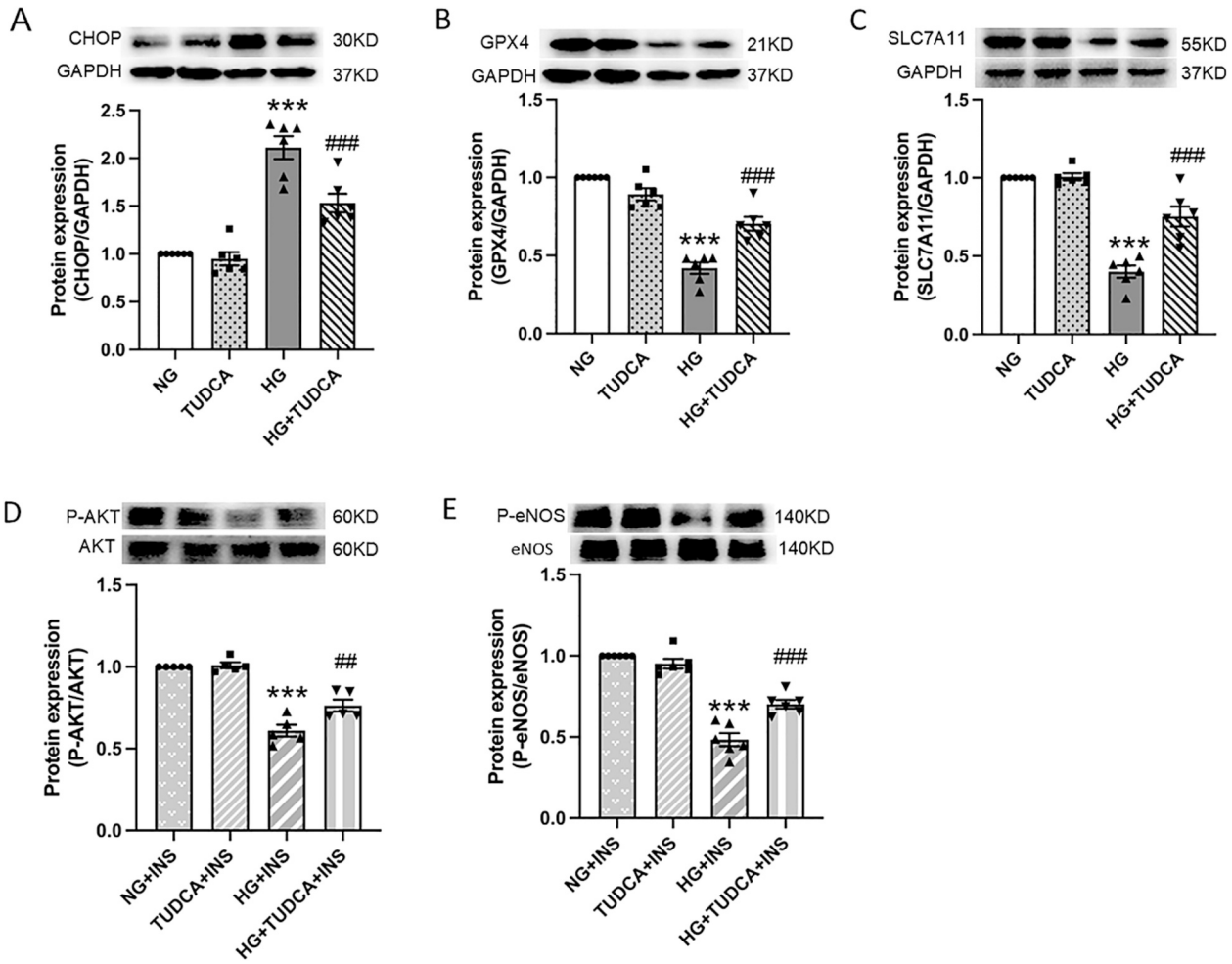


Fig. 8. Inhibition of ER stress by tauroursodeoxycholic acid (TUDCA) attenuates high glucose-induced ferroptosis in HUVECs. Protein expression of CHOP (A), N = 6; GPX4 (B), N = 6; SLC7A11 (C), N = 6; P-AKT Ser473 (D), N = 5, P-eNOS Ser1177 (E), N = 6. ***p<0.001 vs. NG group or NG+INS group; ###p<0.001, ##p<0.01 vs. HG group or HG+INS group.

4. Discussion

The principal findings of this study are that ferroptosis plays a critical role in the pathogenesis of diabetic endothelial injury and endothelial insulin resistance [37]. Using complementary *in vivo* model, we demonstrate that high glucose drives a deleterious cascade wherein oxidative stress initiates ER stress, which in turn promotes ferroptosis, ultimately impairing the endothelial insulin stimulation of AKT/eNOS signaling axis [38]. Crucially, the inhibition of ferroptosis with Fer-1 was sufficient to break this cascade and improved vascular function without altering systemic glycemia, suggesting that ferroptosis represents a direct pathogenic mechanism of diabetic vasculopathy rather than a secondary consequence of hyperglycemia alone [37].

Our *in vivo* experiments established a mechanistic link between ferroptosis and diabetic vasculopathy in *db/db* diabetic mice. The *db/db* mouse exhibited classic features of vascular complications, including aortic remodeling, elevated oxidative stress, and profound impairment of endothelium-dependent vasodilation in response to both acetylcholine and insulin. The amelioration of these structural and functional deficits by Fer-1 strongly implicates ferroptosis as a key driver of diabetic vascular injury. Intriguingly, Fer-1 improved specific metabolic parameters, such as body weight, lipid profile, and SBP, without altering hyperglycemia or glucose intolerance [39]. This dissociation suggests that ferroptosis inhibition confers vascular protection through mechanisms that are at least partially independent of glucose lowering [40]. However, it is important to acknowledge that Fer-1 functions as a lipid radical-trapping antioxidant, and some protective effects may reflect broader suppression of lipid peroxidation and oxidative injury rather than exclusive ferroptosis inhibition [41]. Nevertheless, the consistent restoration of canonical ferroptosis markers, iron homeostasis, and mitochondrial morphology observed in our study, together with complementary genetic manipulation of ER stress signaling, supports a major contribution of ferroptosis to the observed vascular phenotype.

Our cellular experiments confirmed that high glucose is a potent inducer of ferroptosis in endothelial cells, as evidenced by the down-regulation of key anti-ferroptotic proteins, (GPX4, Nrf2, FTH1, SLC7A11), upregulation of pro-ferroptotic markers (4HNE, TFR), labile iron accumulation, and the characteristic mitochondrial damage. The reversal of all these hallmarks by Fer-1 confirms ferroptotic cell death. Impaired system Xc^--GSH-GPX4 function was verified by disrupted glutathione homeostasis. Osmotic and glucose titration controls confirmed hyperglycemia-specific effects. These findings were validated in HMEC-1, supporting mechanistic robustness and broader physiological relevance.

A central question arising from our findings was the interplay between the well-established drivers of diabetic complications: oxidative and ER stress and the more recently characterized process of ferroptosis [26]. Our data support a model where these pathways are not parallel but are intricately linked in a vicious, self-amplifying cycle under high glucose conditions. We identified oxidative stress as a critical upstream initiator of this cascade. The antioxidant NAC was remarkably effective, not only in quenching ROS but also in concomitantly attenuating ER

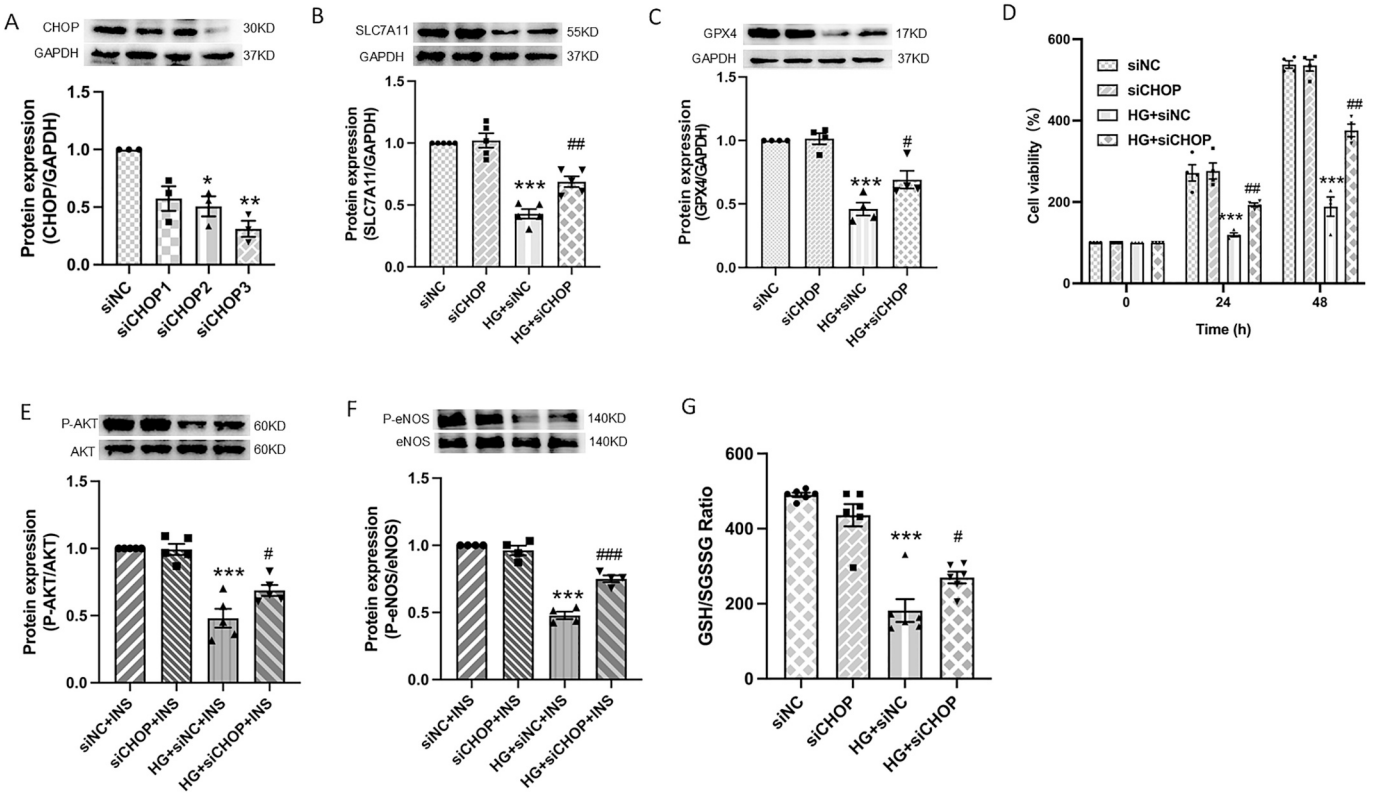


Fig. 9. CHOP silencing attenuates high glucose-induced ferroptosis and restores insulin signaling in HUVECs. (A) Western blot analysis confirming CHOP knockdown efficiency by siRNA, N = 3; (B-C) Protein expression of SLC7A11, N = 5 and GPX4, N = 4. (D) Cell viability, N = 6. P-AKT Ser473 (E), N = 5, P-eNOS Ser1177 (F), N = 4. (G) Cellular GSH/GSSG ratio, N = 6; ***p<0.001, **p<0.01, *p<0.05 vs. siNG group or siNC+INS group; ###p<0.001, ##p<0.01, #p<0.05 vs. HG+siNC group or HG+siNC+INS group.

stress [42], inhibiting ferroptosis [43], restoring glutathione balance, and rescuing insulin signaling. This demonstrates that oxidative stress functions as a primary initiating event rather than merely a downstream consequence of ferroptosis [44].

This interpretation is consistent with the well-established concept that excessive ROS can disrupt protein folding within the ER lumen, thereby activating unfolded protein response pathways [45]. At the same time, our observation that Fer-1 partially reduced ER stress markers suggest the existence of a bidirectional amplification loop in which ferroptosis-associated lipid peroxidation and mitochondrial dysfunction further exacerbate oxidative and ER stress. Thus, we propose a model in which oxidative stress initiates ER stress, which promotes ferroptosis, and ferroptosis feeds back to amplify cellular stress, forming a self-reinforcing pathogenic cycle under hyperglycemic conditions.

Downstream of oxidative stress, we identified ER stress, and specifically the transcription factor CHOP, as a pivotal mediator linking metabolic stress to ferroptosis [46,47]. The ER stress inhibitor TUDCA restored GPX4 and SLC7A11 and improved insulin signaling, indicating that ER stress lies upstream of ferroptotic dysregulation. Among ER stress mediators, the transcription factor CHOP appears to function as a key regulatory node integrating stress signaling with ferroptotic pathways. Genetic silencing of CHOP restored SLC7A11 and GPX4 expression, increased cellular viability, improved glutathione homeostasis, and rescued insulin-stimulated AKT and eNOS phosphorylation. These findings provide causal evidence that CHOP contributes to ferroptosis-associated endothelial dysfunction [48].

Regarding the regulatory relationship between CHOP and SLC7A11, our results are most consistent with an indirect mechanism. Although CHOP knockdown restored SLC7A11 expression, SLC7A11 transcription is primarily governed by activating transcription factor 4 (ATF4) and Nrf2 [49], not direct CHOP promoter binding. As a downstream effector of the protein kinase RNA-like endoplasmic reticulum kinase (PERK)–eukaryotic initiation factor (eIF)2α-ATF4 axis [50], CHOP likely modulates SLC7A11 through heterodimerization with C/EBP members or via broader stress signaling networks, rather than functioning as a direct repressor. Further chromatin immunoprecipitation and promoter analyses are needed to delineate the underlying mechanisms.

We acknowledge that positioning ferroptosis as a convergent mechanism represents a simplified view of a complex cellular stress network. Autophagy, particularly mitophagy, serves as a critical protective mechanism by eliminating damaged mitochondria and preventing ROS accumulation [51]. In diabetes, impaired mitophagy may contribute to mitochondrial dysfunction and vulnerability to ferroptosis [52]. Conversely, dysregulated autophagy can promote ferroptosis through selective degradation of anti-ferroptotic proteins, such as GPX4 and SLC7A11 [53]. The mitochondrial damage observed in our TEM analysis could theoretically trigger mitophagy as a compensatory response. The partial protection conferred by Fer-1 may reflect the contribution of these parallel stress pathways that remain operational despite ferroptosis inhibition. Future studies employing genetic manipulation of autophagy regulators combined with ferroptosis inhibition would help dissect the hierarchical relationship between these interconnected stress responses.

Our study also highlights the functional consequences of ferroptosis on endothelial insulin signaling. The PI3K/AKT/eNOS pathway is central to insulin-mediated nitric oxide production and vascular homeostasis, and its impairment represents a hallmark of endothelial insulin resistance in diabetes [54]. Restoration of AKT and eNOS phosphorylation by both Fer-1 and CHOP silencing provides mechanistic evidence that ferroptosis directly contributes to insulin signaling dysfunction. In vascular reactivity experiments, supraphysiological insulin

concentrations were required to achieve maximal vasodilatory responses [55], which likely reflects reduced insulin sensitivity in diabetic vessels rather than physiological circulating levels. This approach is commonly used in isolated vessel studies to evaluate insulin responsiveness and does not diminish the relevance of the findings [56,57].

Several limitations should be considered when interpreting our results. First, ER stress assessment relied primarily on GRP78 and CHOP protein expression, which may not fully capture functional activation of unfolded protein response pathways. Although CHOP silencing provides functional evidence for ER stress involvement, additional pathway-specific measurements, such as PERK-eIF2α phosphorylation, X-box binding protein1 splicing, or ATF6 activation, would provide more comprehensive mechanistic insight [58]. Second, Fer-1, while used as a ferroptosis inhibitor, functions as a radical-trapping antioxidant [30]. Thus, some protective effects on ER stress and insulin signaling may reflect broader redox modulation rather than ferroptosis-specific inhibition. However, Fer-1 reversed canonical ferroptosis hallmarks, and genetic modulation of the ER stress-CHOP axis produced parallel changes in ferroptosis markers, supporting mechanistic specificity. Third, some experimental endpoints were performed with modest biological sample sizes, which may limit statistical power despite consistent findings across independent assays. Fourth, only male db/db mice were included, representing an important limitation given increasing recognition that sex hormones influence oxidative stress, iron metabolism, ER stress responses, and ferroptosis susceptibility. Estrogen, for example, may exert protective vascular effects by modulating redox balance and GPX4 activity [59]. Therefore, extrapolation of our findings to females should be made with caution, and future studies incorporating sex-specific analyses are warranted. Fifth, while osmotic control experiments were performed in HMEC-1 to confirm glucose specificity, these controls were not conducted in HUVECs, which represent a methodological limitation. Finally, the *db/db* mouse features leptin receptor deficiency, whereas most human T2DM involves leptin resistance. Although widely accepted and reflective of key diabetic vascular complications, validation in complementary models would enhance translational relevance.

In conclusion, this study demonstrates ferroptosis as a critical pathogenic mechanism in diabetic endothelial injury and insulin resistance, and delineates a novel oxidative stress/ER stress/CHOP/ferroptosis axis that disrupts endothelial insulin signaling [24,60]. The ability of Fer-1 to confer significant vascular protection in *db/db* mice without affecting glycemia highlights the therapeutic potential as a complementary strategy to existing anti-diabetic therapies [61]. Future studies incorporating genetic approaches, sex-specific analyses, and clinically relevant disease models will be essential for translating these findings into targeted therapies aimed at preventing or reversing diabetic vascular complications.

CRediT authorship contribution statement

Yue Ma: Investigation, Data curation. **Junjia Gao:** Investigation, Data curation. **Yaqian Sun:** Methodology, Data curation. **Yufan Gu:** Software, Methodology. **Lu Zhang:** Funding acquisition, Data curation. **Yanru Zhen:** Software, Data curation. **Hui Jia:** Investigation, Data curation. **Yueyang Liu:** Writing – original draft, Supervision. **Qian Xu:** Writing – original draft, Funding acquisition. **Ming-Sheng Zhou:** Writing – review & editing, Writing – original draft, Visualization, Supervision, Funding acquisition, Data curation.

Declaration of competing interest

The authors declare that they have no known competing financial interests or personal relationships that could have appeared to influence the work reported in this paper.

Acknowledgements

This work was funded by the National Natural Science Foundation of China (Nos. 81970357, 2019; 82270434, 2022) to Ming-Sheng Zhou, and by Key R&D Project of Liaoning Provincial Department of Science and Technology (2025JH2/101300019), the Research Project of Educational Commission of Liaoning Province (LJ212410164003), and the U35 Outstanding Young Talent Program of Shenyang (RC240612) to Yueyang Liu, Shenyang Medical College Postgraduate Scientific and Technological Innovation Fund Project (Y20240515) to Yufan Gu, and by Key R&D Project of Liaoning Provincial Department of Science and Technology (2024JH2/102500033), Liaoning Provincial Department of Education Research Platform Construction Project (LJ232410164023), Shenyang Science and Technology Bureau Public Health Research and Development Special Project (24-214-3-145) to Junjia Gao, the National Natural Science Foundation of China (82100316) to Lu Zhang.

Data availability

The datasets supporting the conclusions of this article are available in the [Mendeley data] repository, [https://data.mendeley.com/preview/g82vz24cd5?a = fc16b598-13ed-4b6c-9f88-c7dc86e16dad].

References

[1] E. Cecerska-Heryć, W. Engwert, J. Michałów, et al., Oxidative stress markers and inflammation in type 1 and 2 diabetes are affected by BMI, treatment type, and complications, Sci. Rep. 15 (1) (2025) 23605, https://doi.org/10.1038/s41598-025-05818-z.
[2] K.M. Love, E.J. Barrett, S.K. Malin, et al., Diabetes pathogenesis and management: the endothelium comes of age, J. Mol. Cell Biol. 13 (7) (2021) 500–512, https://doi.org/10.1093/jmcb/mjab024.
[3] V. De Nigris, G. Pujadas, L. La Sala, et al., Short-term high glucose exposure impairs insulin signaling in endothelial cells, Cardiovasc. Diabetol. 14 (2015) 114, https://doi.org/10.1186/s12933-015-0278-0.
[4] R. Muniyappa, H. Chen, M. Montagnani, et al., Endothelial dysfunction due to selective insulin resistance in vascular endothelium: insights from mechanistic modeling, Am. J. Physiol. Endocrinol. Metab. 319 (3) (2020) E629–E646, https://doi.org/10.1152/ajpendo.00247.2020.
[5] C. Contreras, A. Sánchez, A. García-Sacristán, et al., Preserved insulin vasorelaxation and up-regulation of the Akt/eNOS pathway in coronary arteries from insulin resistant obese Zucker rats, Atherosclerosis 217 (2) (2011) 331–339, https://doi.org/10.1016/j.atherosclerosis.2011.03.036.
[6] M. Siragusa, B. Fisslthaler, Insulin keeps PYK-ing on eNOS: enhanced insulin receptor signaling induces endothelial dysfunction, Circ. Res. 120 (5) (2017) 748–750, https://doi.org/10.1161/circresaha.117.310576.
[7] S. Prakash, P. Choudhury, S. Bisht, Diabetic cardiomyopathy and COVID-19: intersecting pathways and amplified cardiovascular risk, Front. Pharmacol. 16 (2025) 1683159, https://doi.org/10.3389/fphar.2025.1683159.
[8] E.F. Brutsaert, Complications of Diabetes Mellitus. 2023 2023/10 [cited 2023; Available from: https://www.msdmanuals.com/professional/endocrine-and-metabolic-disorders/diabetes-mellitus-and-disorders-of-carbohydrate-metabolism/complications-of-diabetes-mellitus.
[9] G. Jia, H. Bai, B. Mather, et al., Diabetic vasculopathy: molecular mechanisms and clinical insights, Int. J. Mol. Sci. 25 (2) (2024), https://doi.org/10.3390/ijms25020804.
[10] H.P. Hammes, Pathophysiological mechanisms of diabetic angiopathy, J. Diabetes Complications 17 (2 Suppl) (2003) 16–19, https://doi.org/10.1016/s1056-8727(02)00275-1.
[11] A. Sun, H. Yang, J. Sun, et al., Treatment of T2DM-related inflammation and vascular injury by regulating cellular crosstalk in the islet microenvironment, Front. Endocrinol. (Lausanne) 16 (2025) 1551853, https://doi.org/10.3389/fendo.2025.1551853.
[12] A.D. Mooradian, Cardiomodulatory effects of cardiometabolic and antihyperglycemic medications: the roles of oxidative and endoplasmic reticulum stress, Am. J. Cardiovasc. Drugs 25 (1) (2025) 37–46, https://doi.org/10.1007/s40256-024-00685-x.
[13] S. Mustapha, M. Mohammed, A.K. Azemi, et al., Current status of endoplasmic reticulum stress in type II diabetes, Molecules 26 (14) (2021) 4362, https://doi.org/10.3390/molecules26144362.
[14] J. Luo, L. Huang, A. Wang, et al., Corrigendum: resistin-induced endoplasmic reticulum stress contributes to the impairment of insulin signaling in endothelium, Front. Pharmacol. 9 (2018) 1446, https://doi.org/10.3389/fphar.2018.01446.
[15] C. Ben Dhaou, Z. Al-Yafeai, G.A. Cruz-Marquez, et al., Integrin-specific signaling drives ER stress-dependent atherogenic endothelial activation, Redox Biol. 88 (2025) 103911, https://doi.org/10.1016/j.redox.2025.103911.
[16] J. Tan, X. Li, N. Dou, Insulin resistance triggers atherosclerosis: caveolin 1 cooperates with PKCzeta to block insulin signaling in vascular endothelial cells,

Cardiovasc. Drugs Ther. 38 (5) (2024) 885–893, https://doi.org/10.1007/s10557-023-07477-6.
[17] Y. Yu, Y. Yan, F. Niu, et al., Ferroptosis: a cell death connecting oxidative stress, inflammation and cardiovascular diseases, Cell Death Discovery 7 (1) (2021) 193, https://doi.org/10.1038/s41420-021-00579-w.
[18] W. Yuan, H. Xia, Y. Xu, et al., The role of ferroptosis in endothelial cell dysfunction, Cell Cycle 21 (18) (2022) 1897–1914, https://doi.org/10.1080/15384101.2022.2079054.
[19] S. Zhang, W. Xin, G.J. Anderson, et al., Double-edge sword roles of iron in driving energy production versus instigating ferroptosis, Cell Death Dis. 13 (1) (2022) 40, https://doi.org/10.1038/s41419-021-04490-1.
[20] E.J. Jin, Y. Jo, S. Wei, et al., Ferroptosis and iron metabolism in diabetes: pathogenesis, associated complications, and therapeutic implications, Front. Endocrinol. (Lausanne) 15 (2024) 1447148, https://doi.org/10.3389/fendo.2024.1447148.
[21] C. Zhang, X. Liu, S. Jin, et al., Ferroptosis in cancer therapy: a novel approach to reversing drug resistance, Mol. Cancer 21 (1) (2022) 47, https://doi.org/10.1186/s12943-022-01530-y.
[22] X. Li, M. Fang, X. Liu, et al., Ferroptosis in diabetes mellitus and its complications: overview of clinical and preclinical research, Cell Death Discov 11 (1) (2025) 504, https://doi.org/10.1038/s41420-025-02780-7.
[23] J. Lan, B. Jiang, X. Zhang, et al., CD36-mediated long-chain fatty acids transport in keratinocytes promotes psoriasis-like skin inflammation by increasing mitochondrial ROS, p. S0022–202X(25), 03555–9, J. Invest. Dermatol. (2025), https://doi.org/10.1016/j.jid.2025.10.615.
[24] S. Yousaf, M. Arshad, M. Raza, et al., Targeting mitochondrial damage and ER stress to inhibit ferroptosis in cadmium-induced nephrotoxicity, Toxicol. Rep. 15 (2025) 102082, https://doi.org/10.1016/j.toxrep.2025.102082.
[25] L. Zhang, X. Wang, Nelfinavir triggers ferroptosis by inducing ER stress mediated downregulation of GPX4/GSH system, upregulation of NRF2/HO-1 axis, and mitochondrial impairment in hepatocellular carcinoma cells, Cell Death Discovery 11 (1) (2025) 444, https://doi.org/10.1038/s41420-025-02761-w.
[26] X. Tao, Y. Zhang, J. Pang, et al., ER stress sensor PERK drives ferroptosis by disrupting MAMs-mediated mitochondrial homeostasis and promoting mtROS accumulation in acute myocardial infarction, Pharmacol. Res. 222 (2025) 108029, https://doi.org/10.1016/j.phrs.2025.108029.
[27] J. Li, L. Li, Z. Zhang, et al., Ferroptosis: an important player in the inflammatory response in diabetic nephropathy, Front. Immunol. 14 (2023) 1294317, https://doi.org/10.3389/fimmu.2023.1294317.
[28] D.H. Nam, J.H. Han, T.J. Lee, et al., CHOP deficiency prevents methylglyoxal-induced myocyte apoptosis and cardiac dysfunction, J. Mol. Cell. Cardiol. 85 (2015) 168–177, https://doi.org/10.1016/j.yjmcc.2015.05.016.
[29] P. Malaviya, J. Kumar, R.A. Kowluru, Role of ferroptosis in mitochondrial damage in diabetic retinopathy, Free Radic. Biol. Med. 225 (2024) 821–832, https://doi.org/10.1016/j.freeradbiomed.2024.10.296.
[30] B. Hu, Y. Liu, X. Chen, et al., Ferrostatin-1 protects auditory hair cells from cisplatin-induced ototoxicity in vitro and in vivo, Biochem. Biophys. Res. Commun. 533 (4) (2020) 1442–1448, https://doi.org/10.1016/j.bbrc.2020.10.019.
[31] L. Huang, A. Wang, Y. Hao, et al., Macrophage depletion lowered blood pressure and attenuated hypertensive renal injury and fibrosis, Front. Physiol. 9 (2018) 473, https://doi.org/10.3389/fphys.2018.00473.
[32] H.L. Ren, R. Cai, R. Xue, et al., Growth hormone-releasing hormone agonist attenuates vascular calcification in diabetic db/db mice, Front. Cardiovasc. Med. 10 (2023) 1102525, https://doi.org/10.3389/fcvm.2023.1102525.
[33] Y. Zhang, Y. Qu, R. Cai, et al., Atorvastatin ameliorates diabetic nephropathy through inhibiting oxidative stress and ferroptosis signaling, Eur. J. Pharmacol. 976 (2024) 176699, https://doi.org/10.1016/j.ejphar.2024.176699.
[34] K. Park, A. Mima, Q. Li, et al., Insulin decreases atherosclerosis by inducing endothelin receptor B expression, JCI Insight 1 (6) (2016) e86574, https://doi.org/10.1172/jci.insight.86574.
[35] J. Fu, M.G. Yu, Q. Li, et al., Insulin's actions on vascular tissues: Physiological effects and pathophysiological contributions to vascular complications of diabetes, Mol. Metab. 52 (2021) 101236, https://doi.org/10.1016/j.molmet.2021.101236.
[36] V. Chen, J. Zhang, J. Chang, et al., CD36 restricts lipid-associated macrophages accumulation in white adipose tissues during atherogenesis, Front. Cardiovasc. Med. 11 (2024) 1436865, https://doi.org/10.3389/fcvm.2024.1436865.
[37] E.F. Luo, H.X. Li, Y.H. Qin, et al., Role of ferroptosis in the process of diabetes-induced endothelial dysfunction, World J. Diabetes 12 (2) (2021) 124–137, https://doi.org/10.4239/wjd.v12.i2.124.
[38] J.Y. Duan, X. Lin, F. Xu, et al., Ferroptosis and its potential role in metabolic diseases: a curse or revitalization? Front. Cell Dev. Biol. 9 (9) (2021) 701788 https://doi.org/10.3389/fcell.2021.701788.
[39] Y. Wu, J. Zhou, Dapansutrile regulates mitochondrial oxidative stress and reduces hepatic lipid accumulation in diabetic mice, Curr. Issues Mol. Biol. 47 (3) (2025) 148, https://doi.org/10.3390/cimb47030148.
[40] S. Kim, S.W. Kang, J. Joo, et al., Characterization of ferroptosis in kidney tubular cell death under diabetic conditions, Cell Death Dis. 12 (2) (2021) 160, https://doi.org/10.1038/s41419-021-03452-x.
[41] F. Xiao, D. Li, M. Yu, et al., Ferrostatin-1 protects against early sepsis-induced acute lung injury by suppressing lipid peroxidation-driven NINJ1-mediated DAMP release and neutrophil activation, Redox Biol. 90 (2026) 104004, https://doi.org/10.1016/j.redox.2026.104004.
[42] B. Paul, H. Merta, R. Ugrankar-Banerjee, et al., Paraoxonase-like APMAP maintains endoplasmic-reticulum-associated lipid and lipoprotein homeostasis, pp. 2313–2330 e10, Dev. Cell 60 (17) (2025), https://doi.org/10.1016/j.devcel.2025.04.008.
[43] Y.H. Kim, T. Kim, K.-Y. Ji, et al., A time-dependently regulated gene network reveals that Aspergillus protease affects mitochondrial metabolism and airway epithelial cell barrier function via mitochondrial oxidants, Free Radic. Biol. Med. 185 (2022) 76–89, https://doi.org/10.1016/j.freeradbiomed.2022.04.013.
[44] N. Houstis, E.D. Rosen, E.S. Lander, Reactive oxygen species have a causal role in multiple forms of insulin resistance, Nature 440 (7086) (2006) 944–948, https://doi.org/10.1038/nature04634.
[45] J. Wang, K.A. Pareja, C.A. Kaiser, et al., Redox signaling via the molecular chaperone BiP protects cells against endoplasmic reticulum-derived oxidative stress, Elife 3 (2014) e03496, https://doi.org/10.7554/eLife.03496.
[46] C. Dong, Z. He, W. Liao, et al., CHAC1 mediates endoplasmic reticulum stress-dependent ferroptosis in calcium oxalate kidney stone formation, Adv. Sci. (Weinh.) 12 (10) (2025) e2403992, https://doi.org/10.1002/advs.202403992.
[47] J. Yong, V.S. Parekh, S.M. Reilly, et al., Chop/Ddit3 depletion in beta cells alleviates ER stress and corrects hepatic steatosis in mice, p. eaba9796, Sci. Transl. Med. 13 (604) (2021), https://doi.org/10.1126/scitranslmed.aba9796.
[48] B. Song, D. Scheuner, D. Ron, et al., Chop deletion reduces oxidative stress, improves beta cell function, and promotes cell survival in multiple mouse models of diabetes, J. Clin. Invest. 118 (10) (2008) 3378–3389, https://doi.org/10.1172/jci34587.
[49] L. Che, L. Zhu, L. Zhou, et al., Deciphering sorafenib resistance in hepatocellular carcinoma via ferroptotic mechanisms, Biochim. Biophys. Acta Rev. Cancer 1881 (2) (2026) 189566, https://doi.org/10.1016/j.bbcan.2026.189566.
[50] J. Lu, H. Xu, L. Li, et al., Didang Tang alleviates neuronal ferroptosis after intracerebral hemorrhage by modulating the PERK/eIF2alpha/ATF4/CHOP/GPX4 signaling pathway, Front. Pharmacol. 15 (2024) 1472813, https://doi.org/10.3389/fphar.2024.1472813.
[51] Y. Lu, Z. Li, S. Zhang, et al., Cellular mitophagy: Mechanism, roles in diseases and small molecule pharmacological regulation, Theranostics 13 (2) (2023) 736–766, https://doi.org/10.7150/thno.79876.
[52] Y. Chen, X. Liu, Y. Liu, et al., Mitochondrial quality control in diabetes mellitus and complications: molecular mechanisms and therapeutic strategies, Cell Death Dis. 16 (1) (2025) 652, https://doi.org/10.1038/s41419-025-07936-y.
[53] C. Jin, J. Li, S. Han, et al., HELLS inhibits autophagy-dependent ferroptosis in nasopharyngeal carcinoma by modulating the Nrf2/HO-1/GPX4 pathway, Int. J. Mol. Med. 57 (5) (2026), https://doi.org/10.3892/ijmm.2026.5788.
[54] Q. Yu, F. Gao, X.L. Ma, Insulin says NO to cardiovascular disease, Cardiovasc. Res. 89 (3) (2011) 516–524, https://doi.org/10.1093/cvr/cvq349.
[55] J.C. Ter Maaten, S.J. Bakker, E.H. Serne, et al., Insulin-mediated increases in renal plasma flow are impaired in insulin-resistant normal subjects, Eur. J. Clin. Invest. 30 (12) (2000) 1090–1098, https://doi.org/10.1046/j.1365-2362.2000.00749.x.
[56] Q. Xu, K. Zhuo, R. Cai, et al., Activation of yes-associated protein/PDZ-binding motif pathway contributes to endothelial dysfunction and vascular inflammation in AngiotensinII hypertension, Front. Physiol. 12 (2021) 732084, https://doi.org/10.3389/fphys.2021.732084.
[57] Q. Xu, K. Zhuo, X. Zhang, et al., Oxytocin-induced endothelial nitric oxide dependent vasorelaxation and ERK1/2-mediated vasoconstriction in the rat aorta, Korean J. Physiol. Pharmacol. 26 (4) (2022) 255–262, https://doi.org/10.4196/kjpp.2022.26.4.255.
[58] A.M. Merlot, N.H. Shafie, Y. Yu, et al., Mechanism of the induction of endoplasmic reticulum stress by the anti-cancer agent, di-2-pyridylketone 4,4-dimethyl-3-thiosemicarbazone (Dp44mT): Activation of PERK/eIF2alpha, IRE1alpha, ATF6 and calmodulin kinase, Biochem. Pharmacol. 109 (2016) 27–47, https://doi.org/10.1016/j.bcp.2016.04.001.
[59] Y. Lv, S. Zhang, X. Weng, et al., Estrogen deficiency accelerates postmenopausal atherosclerosis by inducing endothelial cell ferroptosis through inhibiting NRF2/GPX4 pathway, FASEB J. 37 (6) (2023) e22992, https://doi.org/10.1096/fj.202300083R.
[60] H.M. Saad, E.A. Salem, O. Elhussieny, et al., Crosstalk between ferroptosis and miRNA in type 2 diabetes mellitus and possible therapeutic targeting, Eur. J. Med. Res. 30 (1) (2025) 982, https://doi.org/10.1186/s40001-025-03178-y.
[61] D. Xie, K. Li, R. Feng, et al., Ferroptosis and traditional chinese medicine for type 2 diabetes mellitus, Diabetes Metab. Syndr. Obes. 16 (2023) 1915–1930, https://doi.org/10.2147/dmso.S412747.